Supplementary Information (SI) for Journal of Materials Chemistry A.
This journal is © The Royal Society of Chemistry 2025

Supporting Information

Stable oxygen reduction catalysts for enhancing rechargeability for zinc–air batteries: FeCoCu nanoparticles embedded in N-doped carbon matrices

Wen Zhao[1], Tianli Wu[2,], Inosh Prabasha Perera[3], Yanliu Dang[4], Isaac T Olowookere[3], Qiang Luo[3], Haiyan Tan[4], Dilshan Silva[3], and Steven L. Suib[1,3,4,*]*

1. Department of Materials Science and Engineering, University of Connecticut, 25 King Hill Rd Unit 3136, Storrs, Connecticut 06269-3136, United States

2. Henan Key Laboratory of Quantum Materials and Quantum Energy, School of Future Technology, Henan University, Kaifeng 475004, China

3. Department of Chemistry, University of Connecticut, 55 N. Eagleville Rd., Storrs, Connecticut 06269-3060, United States

4. Institute of Materials Science, University of Connecticut, 25 King Hill Rd Unit 3136, Storrs, Connecticut 06269-3136, United States

* Corresponding Authors.

Email: steven.suib@uconn.edu, tianliwu@henu.edu.cn

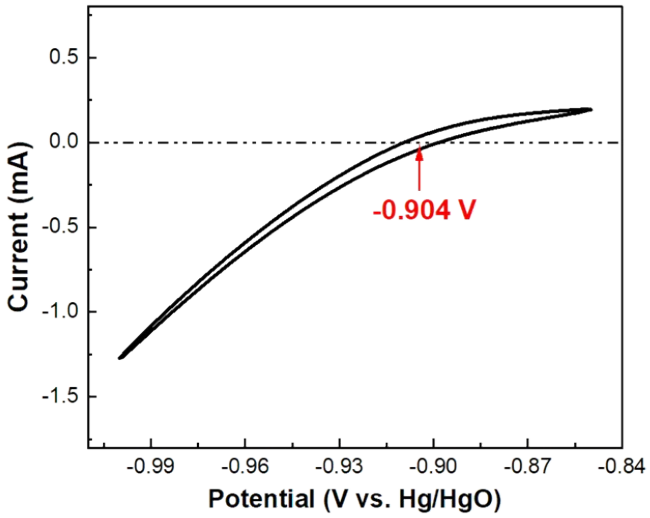

Fig. S1 RHE calibration of the Hg/HgO reference electrode in 0.1 M KOH.

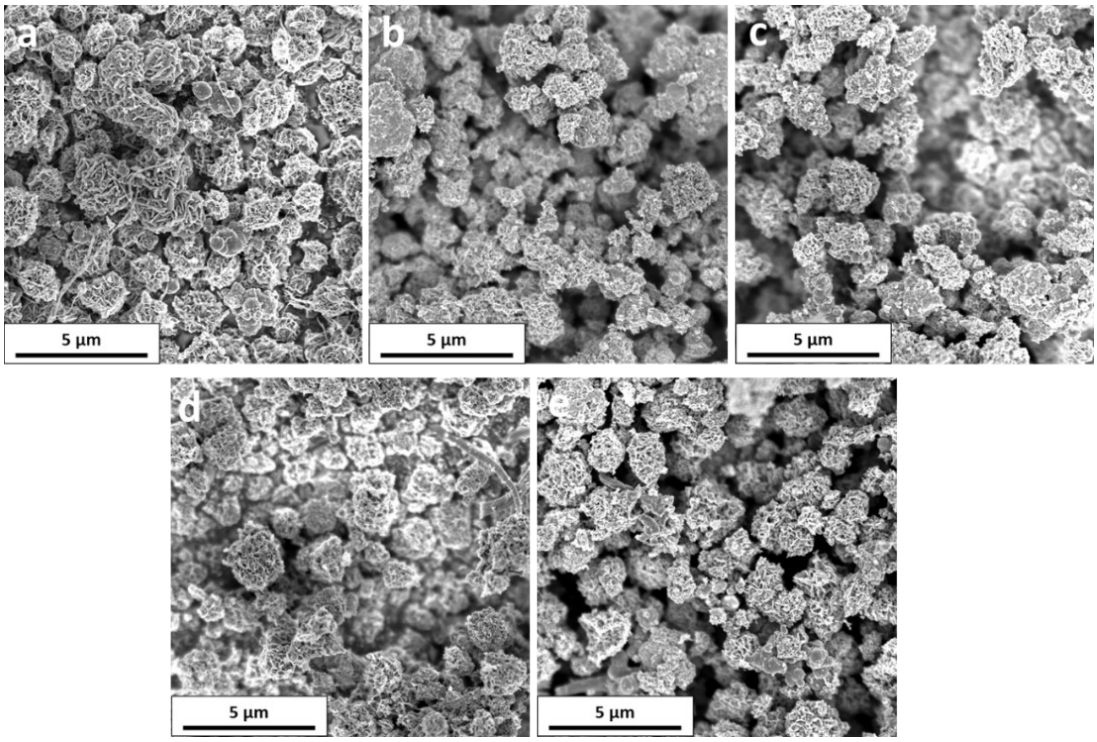

Fig. S2 SEM image of (a) N-doped carbon/FeCo, (b) N-doped carbon/FeCoCu-2, (c) N-doped carbon/FeCoCu-10, (d) N-doped carbon/FeCoCu-15 and (e) N-doped carbon/FeCoCu-20.

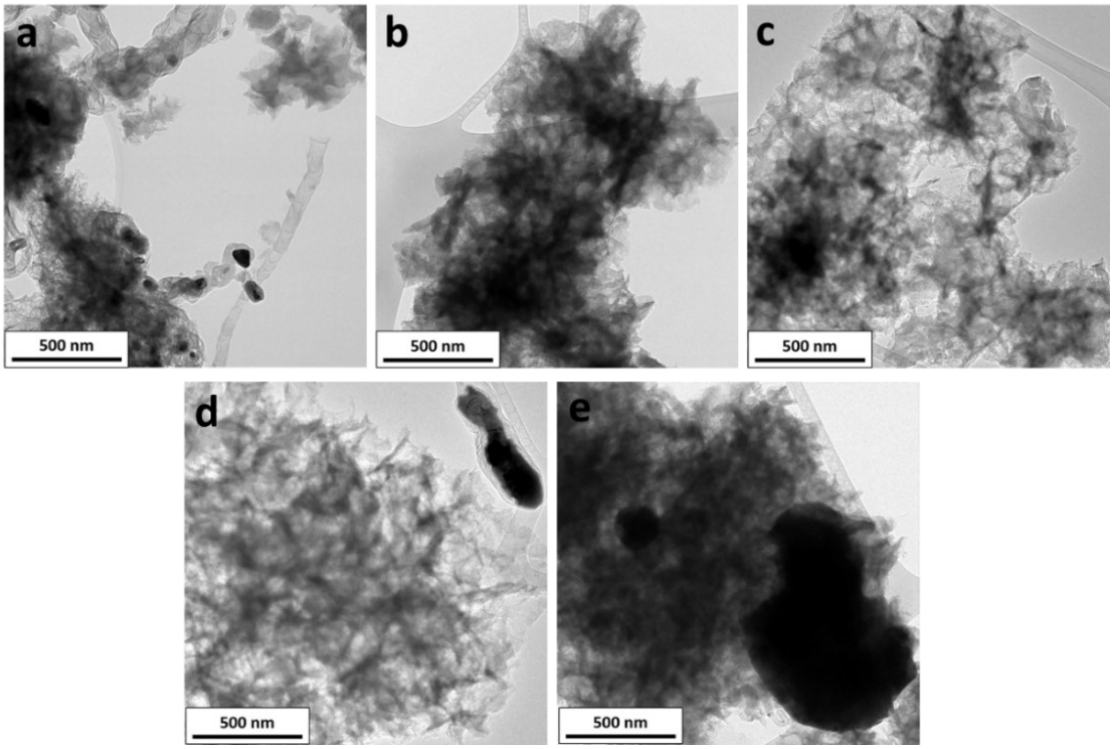

Fig. S3 TEM image of (a) N-doped carbon/FeCo, (b) N-doped carbon/FeCoCu-2, (c) N-doped carbon/FeCoCu-10, (d) N-doped carbon/FeCoCu-15 and (e) N-doped carbon/FeCoCu-20.

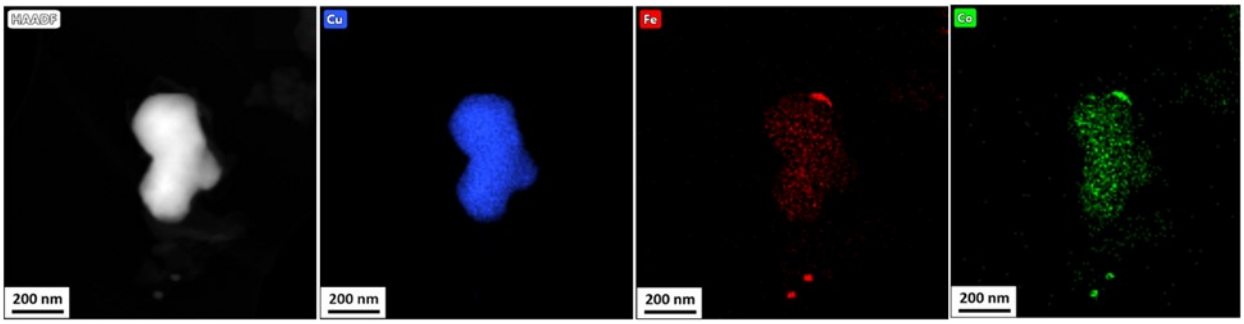

Fig. S4 HAADF-STEM image and corresponding EDS elemental mappings of N-doped carbon/FeCoCu-15. The EDS elemental mappings reveal that Cu (blue) is predominantly distributed throughout the particle, whereas Fe (red) and Co (green) are confined to a limited portion on the edge of the particle.

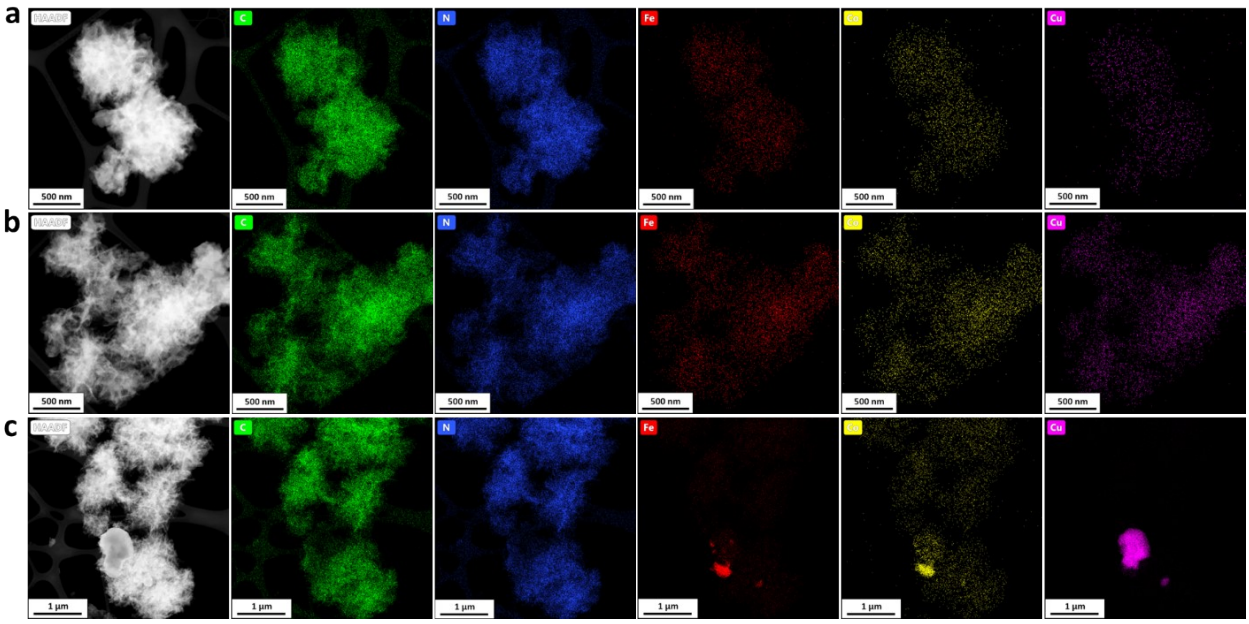

Fig. S5 HAADF-STEM image and corresponding EDS elemental mappings of (a) N-doped carbon/FeCoCu-2, (b) N-doped carbon/FeCoCu-10 and (c) N-doped carbon/FeCoCu-20.

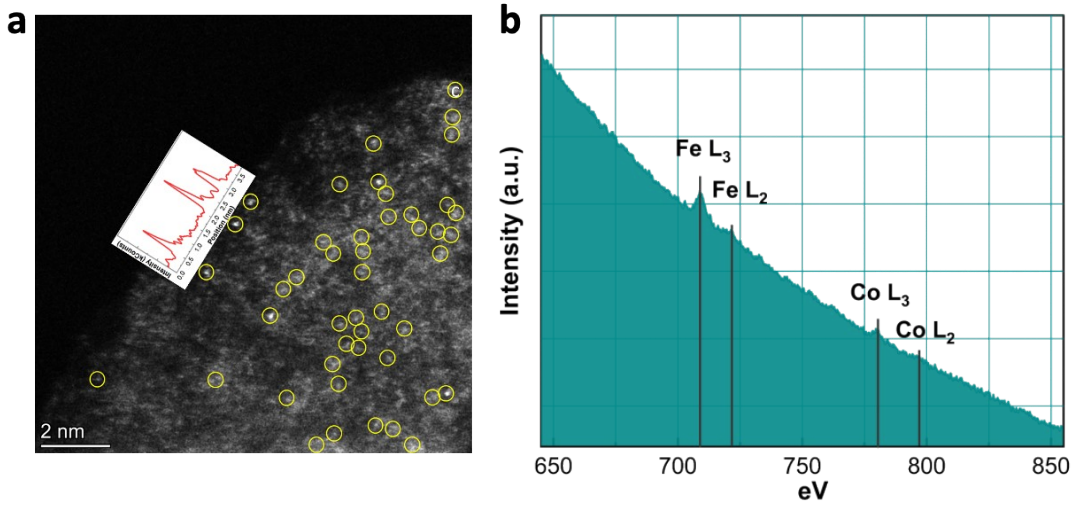

Fig. S6 HAADF-STEM images displaying single atoms dispersed in carbon with the intensity profile (inset) and (b) EELS spectrum of N-doped carbon/FeCoCu-2.

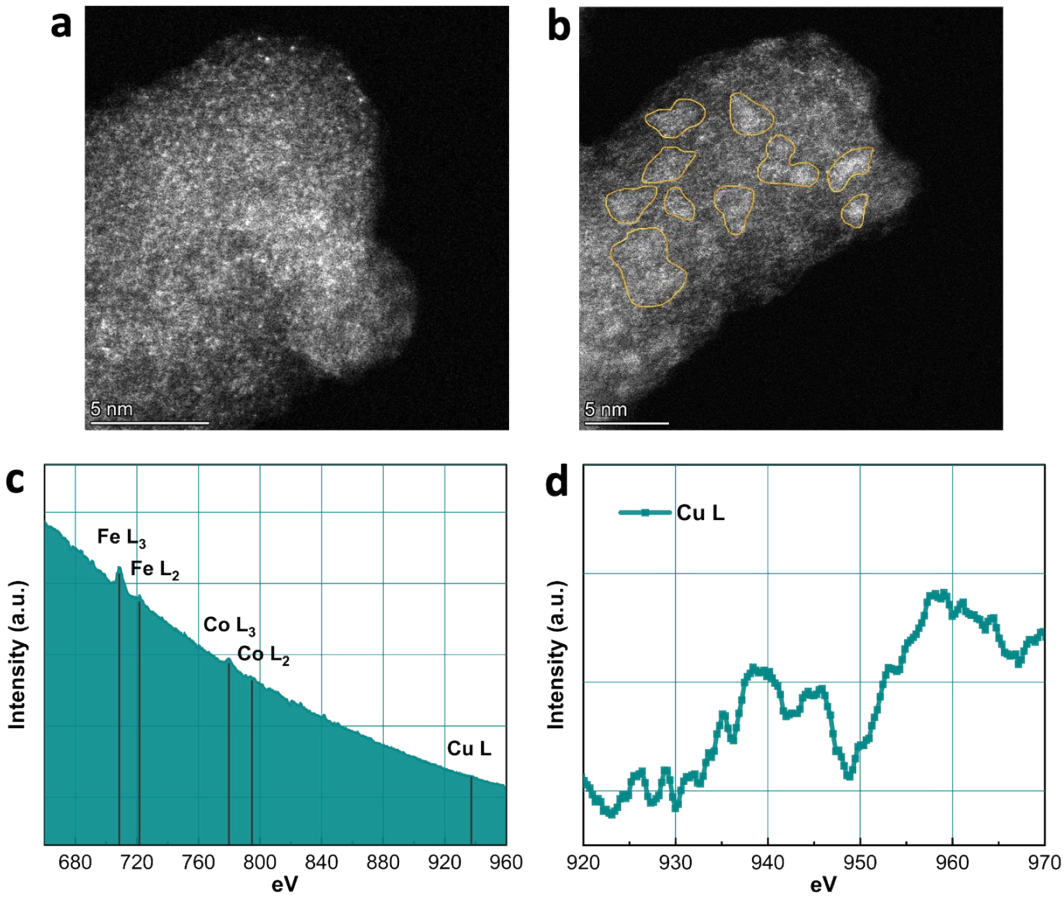

Fig. S7 HAADF-STEM images showing (a) single atoms dispersed in a carbon matrix and (b) atom clusters. (c) EELS spectrum and (d) magnified Cu L peaks of N-doped carbon/FeCoCu-10.

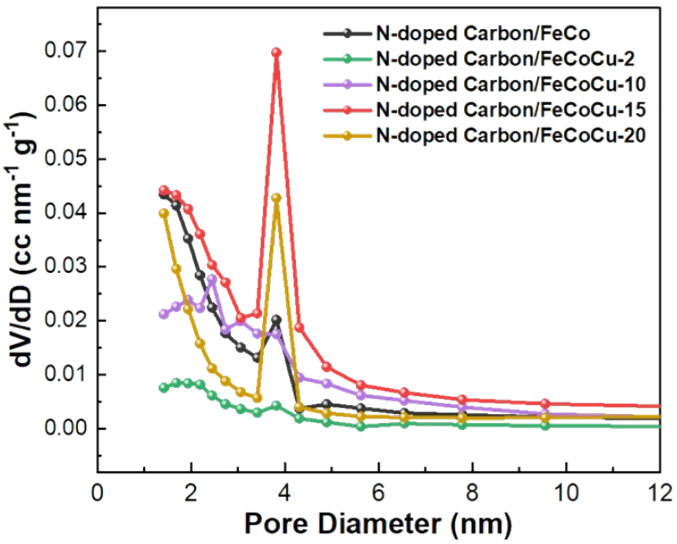

Fig. S8 Pore size distributions of as-prepared catalysts.

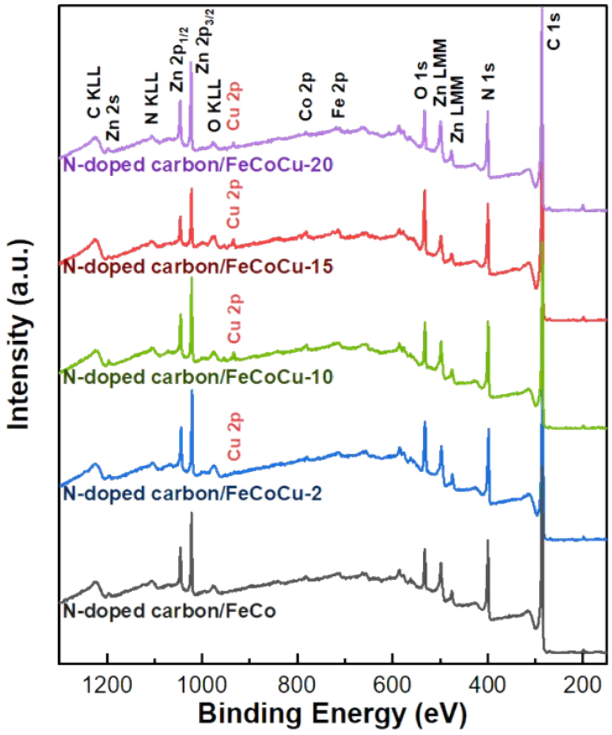

Fig. S9 Full-survey XPS spectra of as-prepared catalysts.

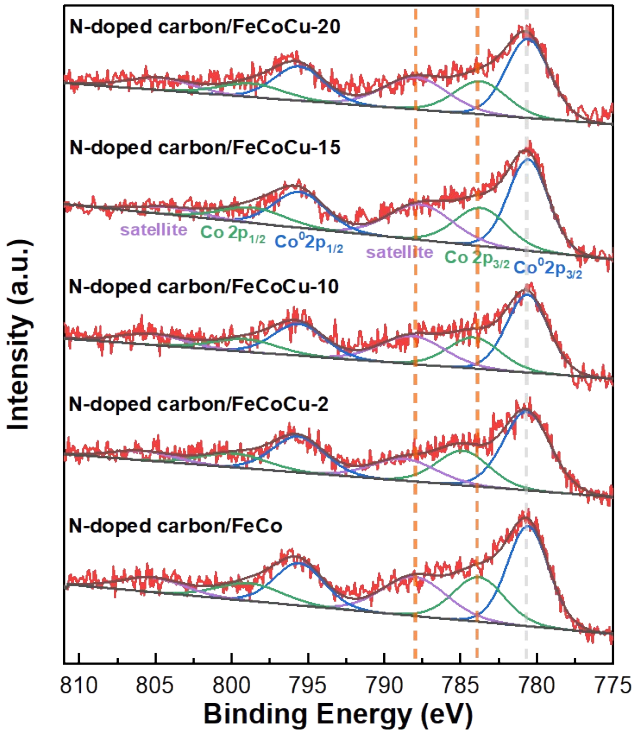

Fig. S10 High-resolution XPS spectra Co 2p for N-doped carbon/FeCo and N-doped carbon/FeCoCu Samples.

Table S1 Elemental composition analysis via high-resolution XPS spectra.

Sample Name	C (at. %)	N (at. %)	O (at. %)	Fe (at. %)	Co (at. %)	Cu (at. %)
N-doped carbon/FeCo	74.91	17.43	6.70	0.54	0.42	–
N-doped carbon/FeCoCu-2	75.91	14.76	8.62	0.35	0.28	0.08
N-doped carbon/FeCoCu-10	73.77	17.44	7.57	0.48	0.32	0.42
N-doped carbon/FeCoCu-15	78.70	11.65	8.30	0.53	0.39	0.43
N-doped carbon/FeCoCu-20	77.26	14.99	6.78	0.36	0.36	0.24

The (–) symbol signifies that the element is not detected.

Table S2 XPS analysis results for high-resolution N 1s spectra of as-prepared samples.

Sample Name	Pyridinic N (at. %) 398.5 eV	Metal-N (at. %) 399.8 eV	Pyrrolic (at. %) 400.9eV	Quaternary N (at. %) 402.6 eV	Oxidized N (at. %) 404.2 eV
N-doped carbon/FeCo	57.0	17.1	20.0	4.1	1.7
N-doped carbon/FeCoCu-2	65.9	4.3	23.8	4.2	1.9
N-doped carbon/FeCoCu-10	59.3	15.9	19.3	3.7	1.8
N-doped carbon/FeCoCu-15	54.8	21.4	18.6	3.5	1.7
N-doped carbon/FeCoCu-20	59.5	17.7	18.5	3.2	1.1

Table S3 XPS analysis results for high-resolution C 1s spectra of as-prepared samples.

Sample Name	C–C (at. %) 248.8 eV	C–N (at. %) 286.1 eV	C=O (at. %) 287.6 eV	–COO (at. %) 289.2 eV	π– π* (at. %) 290.9 eV
N-doped carbon/FeCo	64.9	21.8	5.6	4.7	3.0
N-doped carbon/FeCoCu-2	62.5	24.2	5.2	4.6	3.5
N-doped carbon/FeCoCu-10	64.2	22.1	5.9	4.6	3.2
N-doped carbon/FeCoCu-15	64.3	21.8	5.8	4.4	3.7
N-doped carbon/FeCoCu-20	67.2	19.9	5.7	4.3	2.9

Table S4. XPS analysis results for high-resolution Fe 2p spectra of as-prepared samples.

Sample Name	Fe^0 $2p_{3/2}$	Fe $2p_{3/2}$	Satellite	Fe^0 $2p_{1/2}$	Fe $2p_{1/2}$	Satellite
N-doped carbon/FeCo	710.67	714.88	719.02	723.77	727.98	732.12
N-doped carbon/FeCoCu-2	710.60	714.77	718.92	723.70	727.87	732.02
N-doped carbon/FeCoCu-10	710.63	714.61	719.05	723.73	727.71	732.15
N-doped carbon/FeCoCu-15	710.80	715.15	719.79	723.90	728.25	732.89
N-doped carbon/FeCoCu-20	710.75	714.97	719.73	723.85	728.07	732.83

Table S5. XPS analysis results for high-resolution Co 2p spectra of as-prepared samples.

Sample Name	Co^0 $2p_{3/2}$	Co $2p_{3/2}$	Satellite	Co^0 $2p_{1/2}$	Co $2p_{1/2}$	Satellite
N-doped carbon/FeCo	780.58	783.80	788.04	795.69	798.80	805.22
N-doped carbon/FeCoCu-2	780.65	784.83	788.70	795.65	799.83	805.88
N-doped carbon/FeCoCu-10	780.60	784.10	788.17	795.60	799.10	805.31
N-doped carbon/FeCoCu-15	780.57	783.66	787.64	795.57	798.66	804.16
N-doped carbon/FeCoCu-20	780.58	783.70	787.96	795.58	798.70	804.76

In high-resolution Co 2p XPS spectra, N-doped carbon/FeCo exhibits zero-valence states for Co (780.6 and 795.7 eV), along with oxidized valence states at 783.8 and 798.8 eV, accompanied by satellite peaks at 788.0 and 805.2 eV. In N-doped carbon/FeCoCu-2 and N-doped carbon/FeCoCu-10, higher oxidized valence states than those in N-doped carbon/FeCo are observed at increased binding energies. Conversely, N-doped carbon/FeCoCu-15 and N-doped carbon/FeCoCu-20 exhibit lower binding energies for oxidized Co states and their satellites, suggesting a smaller valence state of Co compared to N-doped carbon/FeCoCu-2, and N-doped

carbon/FeCoCu-10. These valence state variations align with the NMR spectra, which indicate that Co-N-C bonding occurs in samples with low Cu concentrations, leading to a higher oxidation state. In contrast, Co bonds with electron-donating Cu atoms in samples with high Cu concentrations, resulting in a lower oxidation state.

Table S6 ORR activity comparison of N-doped carbon/FeCoCu, commercial Pt/C, and other reported ORR electrocatalysts in 0.1 M KOH.

Catalyst	**Mass Loading (mg cm^{-2})**	**Onset Potential (V vs. RHE)**	**$E_{1/2}$ (V vs. RHE)**	**$J_{Limiting}$ (mA cm^{-2})**	**J_K at 0.85V (mA cm^{-2})**	**Ref.**
Pt/C	0.63	0.890	0.807	5.66	3.47	
N-doped carbon/FeCo		0.880	0.820	5.64	2.80	This work
N-doped carbon/FeCoCu-2		0.850	0.800	4.83	0.77	
N-doped carbon/FeCoCu-10		0.870	0.815	4.98	1.86	
N-doped carbon/FeCoCu-15		0.910	0.852	5.62	16.44	
N-doped carbon/FeCoCu-20		0.894	0.839	5.20	6.49	
CoO-TiO_2@NG	0.42	–	0.850	4.85	–	[1]
MnO/NC	0.27	0.850	0.740	5.89	–	[2]
NiCo/Co-NiO/rGO	0.26	–	0.850	5.74	–	[3]
ZnSe@PNCs-1000	0.50	1.040	0.905	5.55	13.62	[4]
Co NPs/N-doped carbon	0.40	0.919	0.859	5.10	–	[5]
MoC@C	–	0.880	0.780	5.85	6.12	[6]
Cu−N−C	0.77	–	0.850	–	5.92	[7]
FeMn-NrGO	–	0.960	0.840	–	–	[8]
Ni–Co–Mn phosphide	–	0.850	0.760	–	–	[9]
Fe_3C|Fe–N–C	0.42	0.961	0.848	5.17	–	[10]
(Fe, Ni)@N-MWCNTs	0.46	0.817	0.732	3.94	–	[11]
CoP/CoO@MNC-CNT	–	0.910	0.838	6.28	–	[12]

The (–) symbol signifies that the information has not been reported.

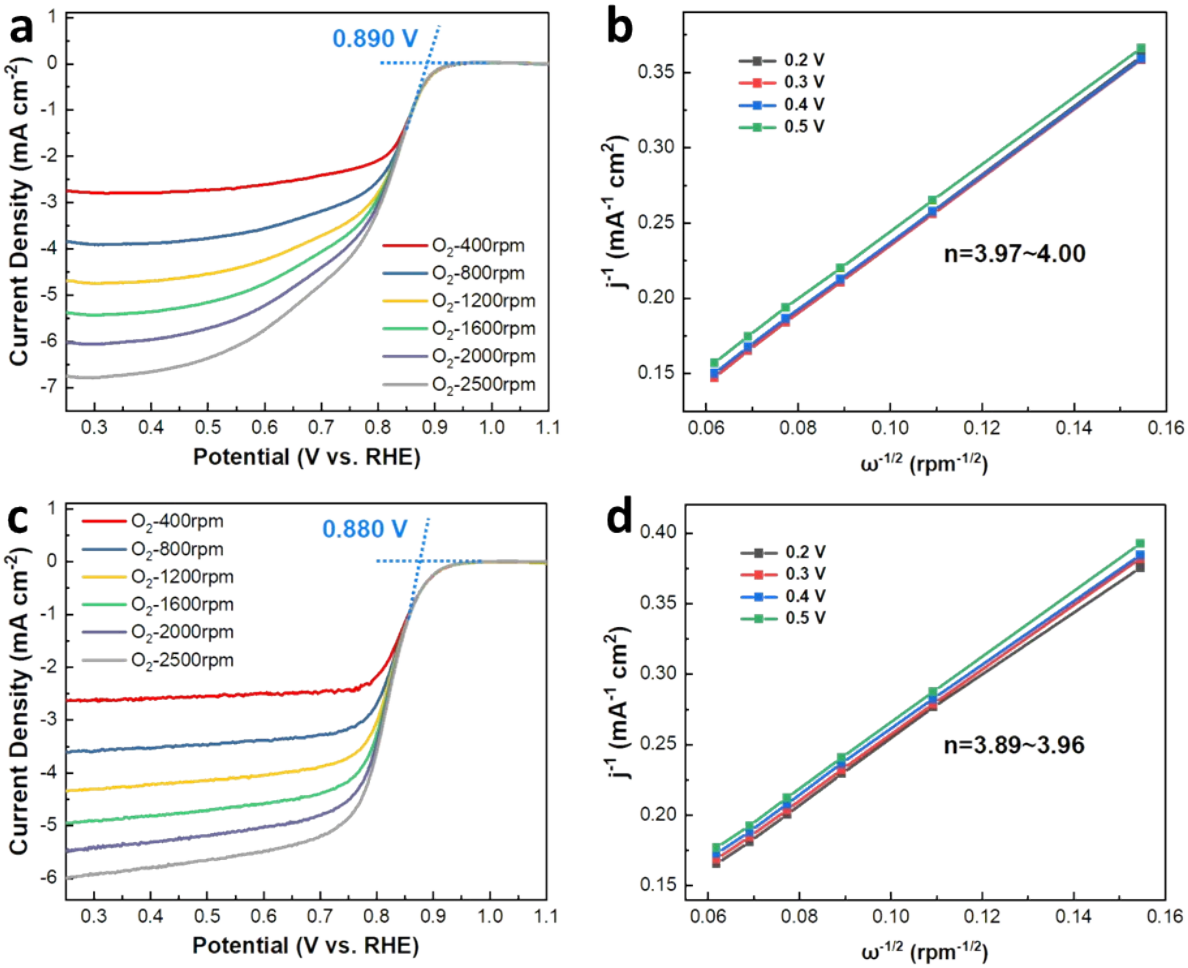

Fig. S11 LSV curves and K-L plots of (a, b) Pt/C, and (c, d) N-doped carbon/FeCo.

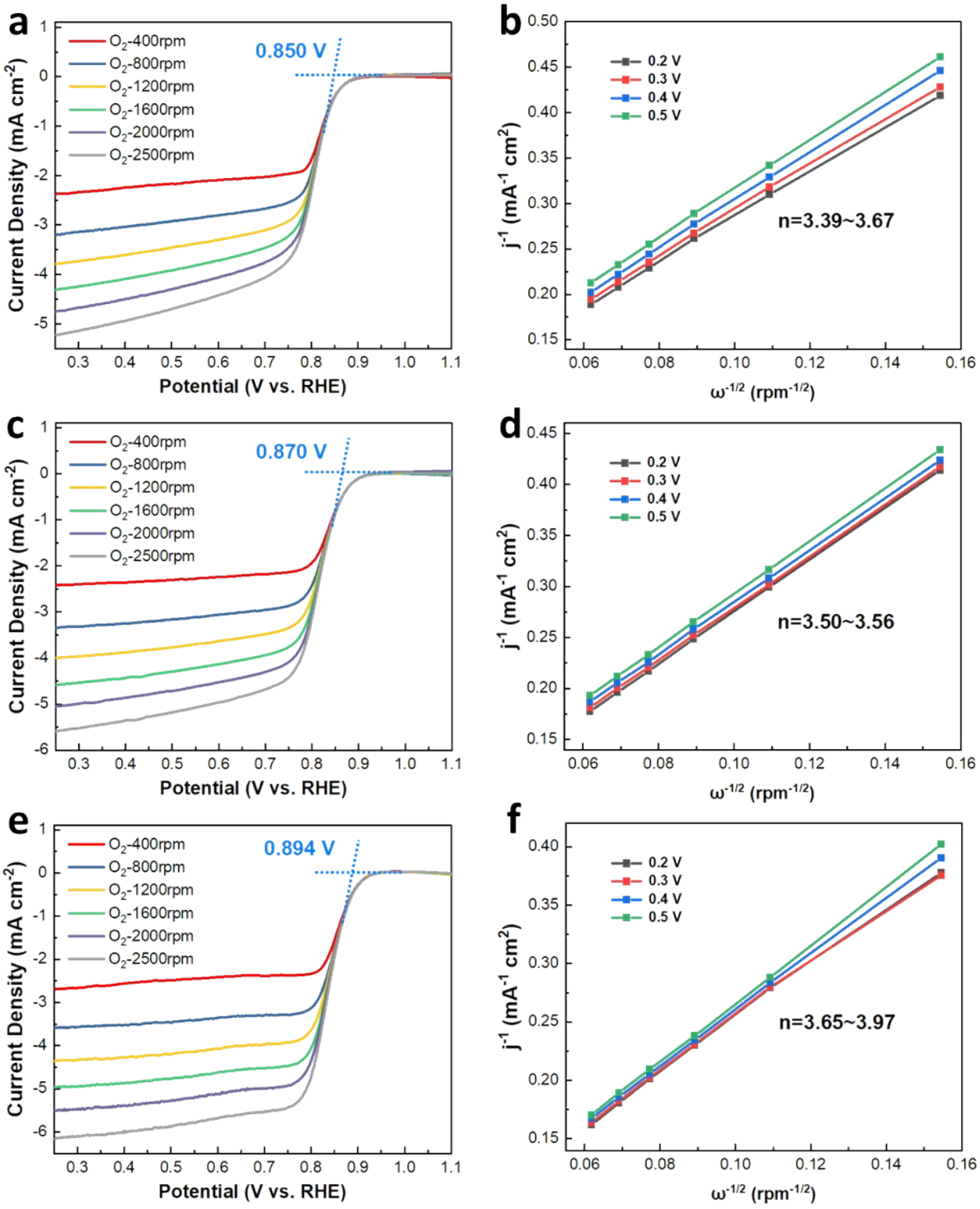

Fig. S12 LSV curves and K-L plots of (a, b) N-doped carbon/FeCoCu-2, (c, d) N-doped carbon/FeCoCu-10 and (e, f) N-doped carbon/FeCoCu-20.

The electron transfer number (n) per oxygen molecule in an ORR process was calculated by the Koutecky-Levich (K-L) equation:

$$J^{-1} = J_k^{-1} + J_L^{-1} = J_k^{-1} + (B\omega^{1/2})^{-1}$$

$$B = 0.62nFC_0D_0^{2/3}v^{-1/6}$$

where J is the measured current density, J_k is the kinetic current density, J_L is the diffusion-limited current density, ω is the electrode rotation angular velocity ($\omega = 2\pi N$, N is the linear rotation speed), B is determined from the slop of K-L plots, F is the Faraday constant (96485 C mol^{-1}), C_0 is the bulk concentration of O_2 (1.2×10^{-6} mol cm^{-3}), D_0 is the diffusion coefficient of O_2 in 0.1 M KOH (1.9×10^{-5} cm^2 s^{-1}), v is the kinetic viscosity (0.01 cm^2 s^{-1}).

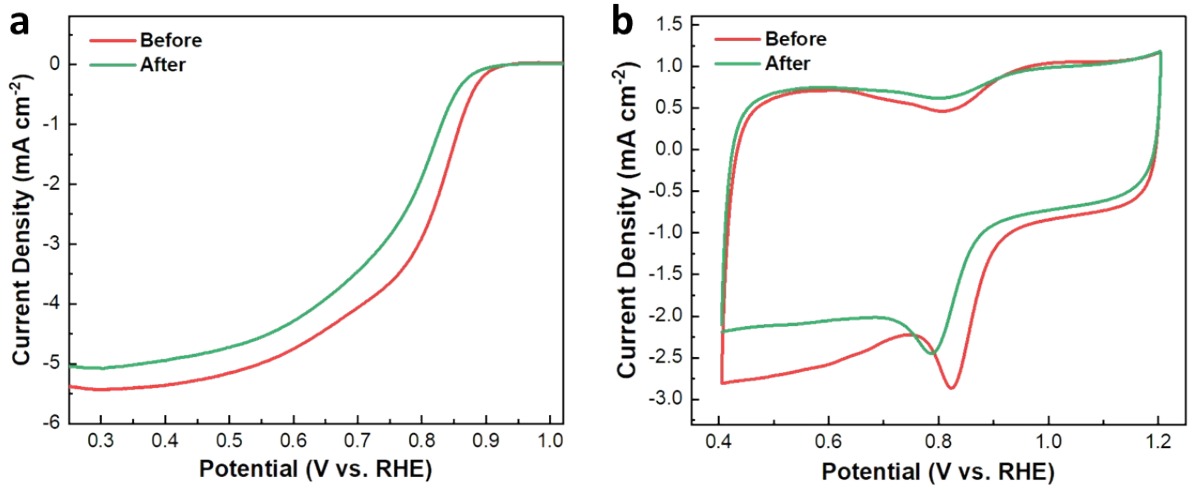

Fig. S13 (a) LSV curves at rotation speed of 1600 rpm and (b) CV curves of Pt/C measured before and after 10 hours stability test.

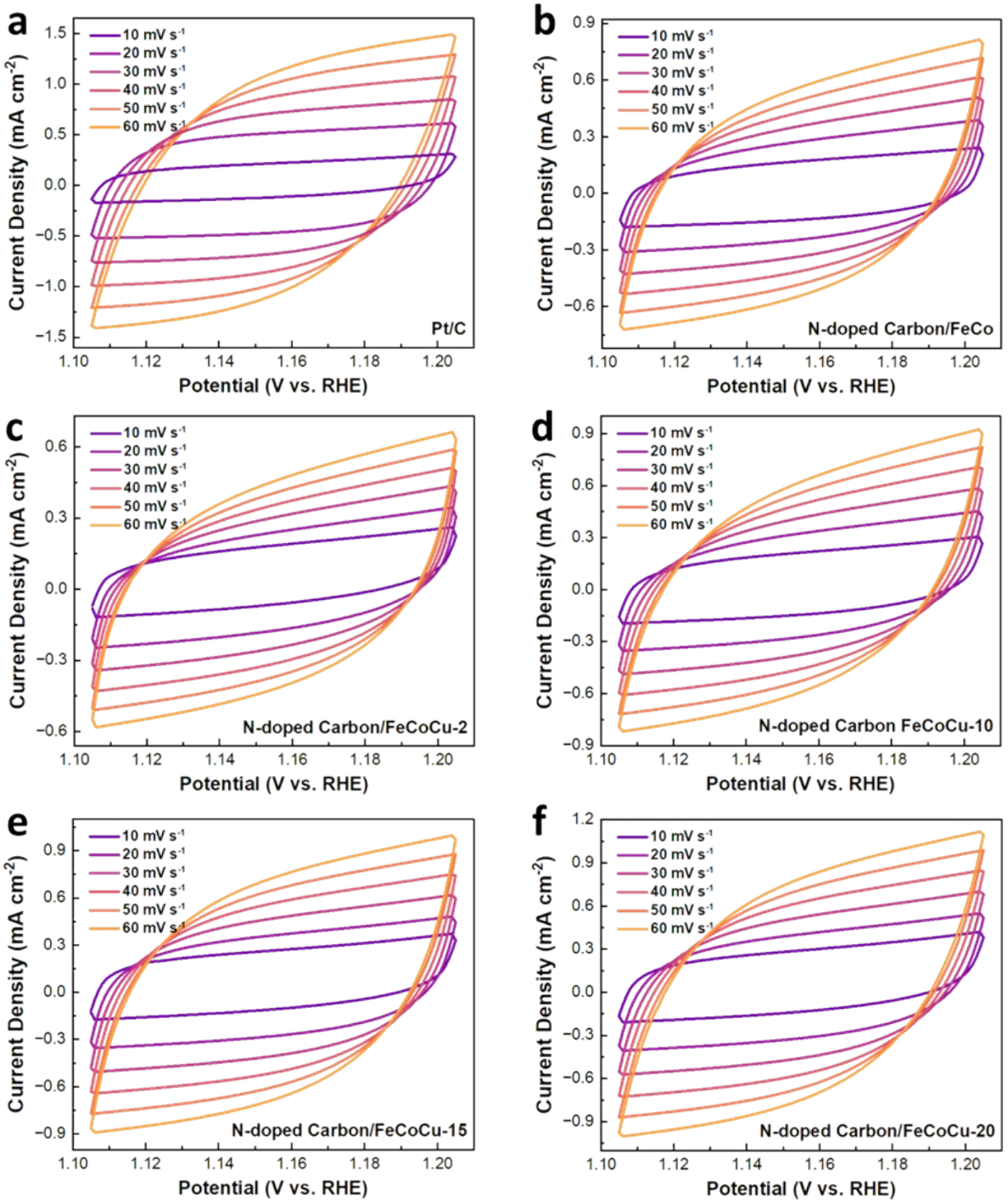

Fig. S14 CV curves for (a) Pt/C, (b) N-doped carbon/FeCo, (c) N-doped carbon/FeCoCu-2, (d) N-doped carbon/FeCoCu-10, (e) N-doped carbon/FeCoCu-15 and (f) N-doped carbon/FeCoCu-20 at different scan rates within a non-Faradaic potential range in a 0.1 M KOH solution.

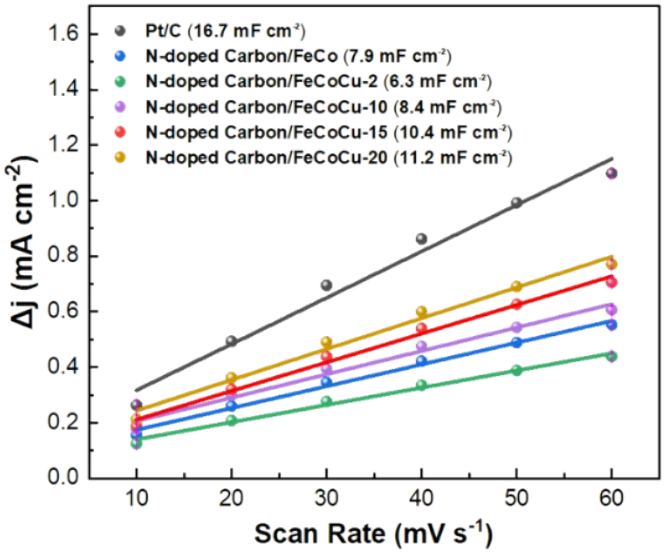

Fig. S15 The electrochemical double-layer capacitance calculated by fitting the CV curves of the catalysts in a 0.1 M KOH solution.

To investigate the intrinsic ORR activity of the prepared catalysts, an assessment of the electrochemically active surface area (ECSA) was carried out using electrochemical double-layer capacitance (C_{dl}). CV measurements were conducted on a rotating electrode in a potential window of 1.125-1.225 V vs. RHE, with scan rates ranging from 10.0 to 60.0 mV s^{-1} (Fig. S12). The C_{dl} was determined by analyzing the slope of the linear fit of half of the charging and discharging current density differences ($\Delta j = \frac{j_c - j_d}{2}$ at a potential of 1.175 V vs. RHE) against the scan rate. As depicted in the Fig. S13, the electrochemical double-layer capacitance (C_{dl}) of N-doped carbon/FeCoCu-15 is calculated to be 10.4 mF cm^{-2}, surpassing that of N-doped carbon/FeCo (7.9 mF cm^{-2}), N-doped carbon/FeCoCu-2 (6.3 mF cm^{-2}), and N-doped carbon/FeCoCu-10 (8.4 mF cm^{-2}), albeit slightly smaller than that of N-doped carbon/FeCoCu-20 (11.2 mF cm^{-2}).

The catalytic activity of the as-prepared materials was evaluated using Turnover Frequency (TOF), calculated as follows:

$$TOF = \frac{I}{nFN}$$

where I is the current measured at a specific potential (A), n is the number of electrons transferred per molecule (typically 4 for ORR), F is the Faraday constant (96485 C·mol^{-1}), and N represents the number of active sites (mol), determined from XPS results.

Table S7 TOF calculation results of as-prepared catalysts and Pt/C.

	Current at 0.8 V (mA cm^{-2})	n	F (C mol^{-1})	Active site (mol cm^{-2})	TOF (s^{-1})
Pt/C	-2.66	4	96485	6.45E-07	0.0107
N-doped carbon/FeCo	-2.92	4	96485	4.63E-07	0.0163
N-doped carbon/FeCoCu-2	-1.97	4	96485	3.44E-07	0.0148
N-doped carbon/FeCoCu-10	-2.58	4	96485	5.80E-07	0.0115
N-doped carbon/FeCoCu-15	-4.22	4	96485	6.43E-07	0.0170
N-doped carbon/FeCoCu-20	-3.68	4	96485	4.64E-07	0.0206

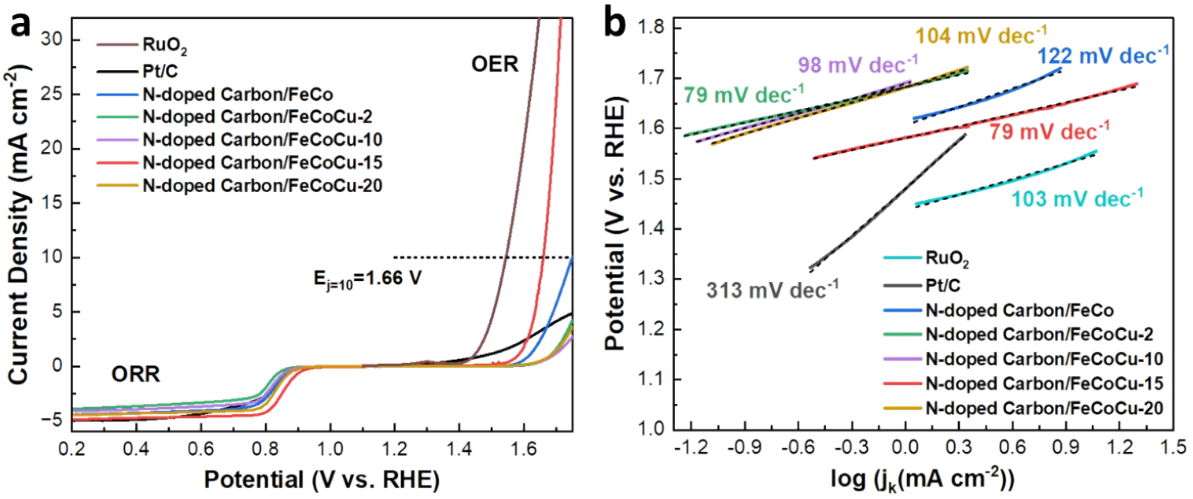

Fig. S16 (a) LSV curves for both ORR and OER of Pt/C, RuO_2, and the prepared catalysts. (b) Tafel slops of Pt/C, RuO_2, and the prepared catalysts.

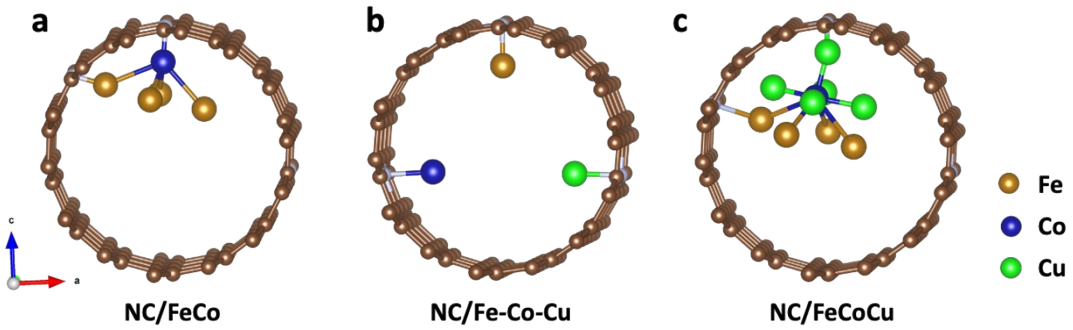

Fig. S17 Structure models of (a) N-doped carbon/FeCo, (b) N-doped carbon/Fe-Co-Cu, and (c) N-doped carbon/FeCoCu.

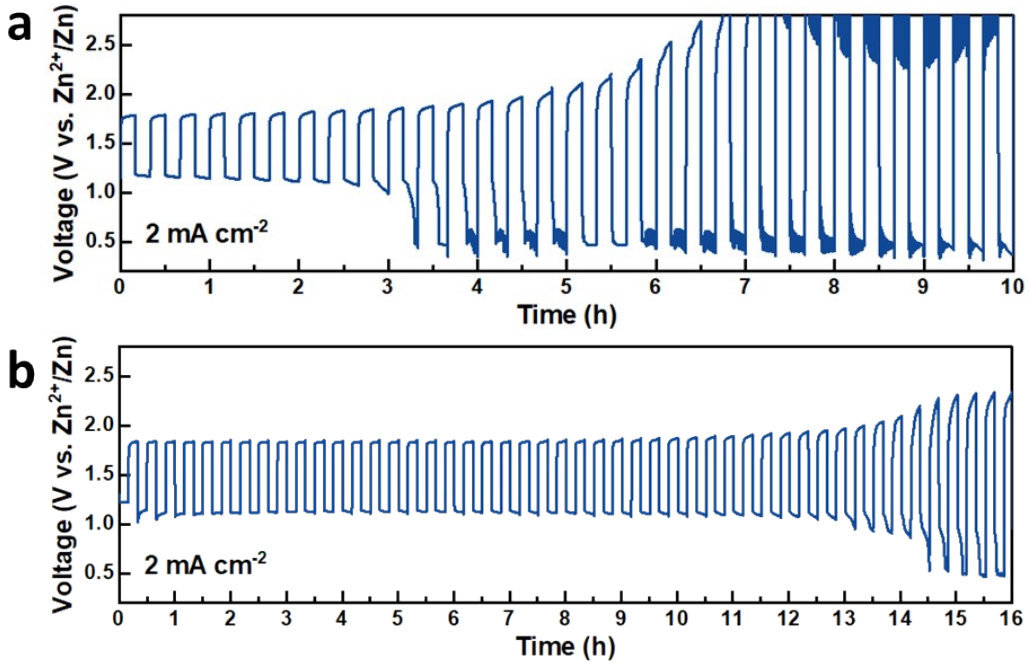

Fig. S18 Galvanostatic cycling curves of coin cells using (a) N-doped carbon/FeCoCu as bifunctional catalyst and (b) a mix of N-doped carbon/FeCoCu and RuO_2 as catalyst in air cathode.

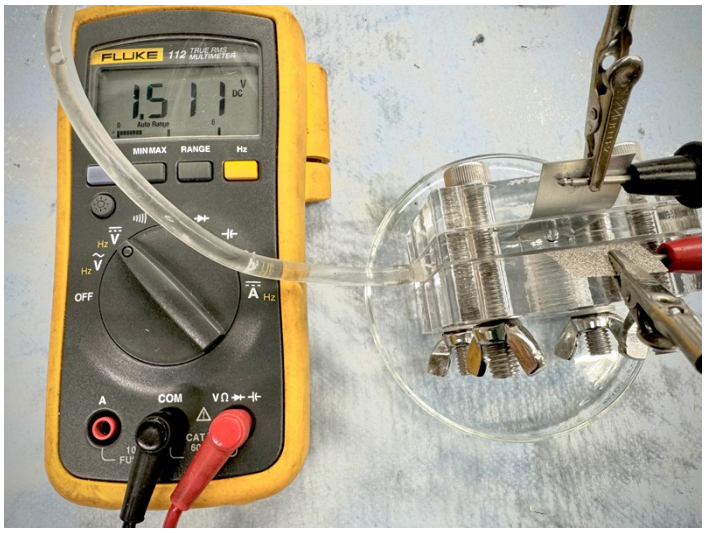

Fig. S19 Photographic image of the voltage meter showing the OCV of ZABs.

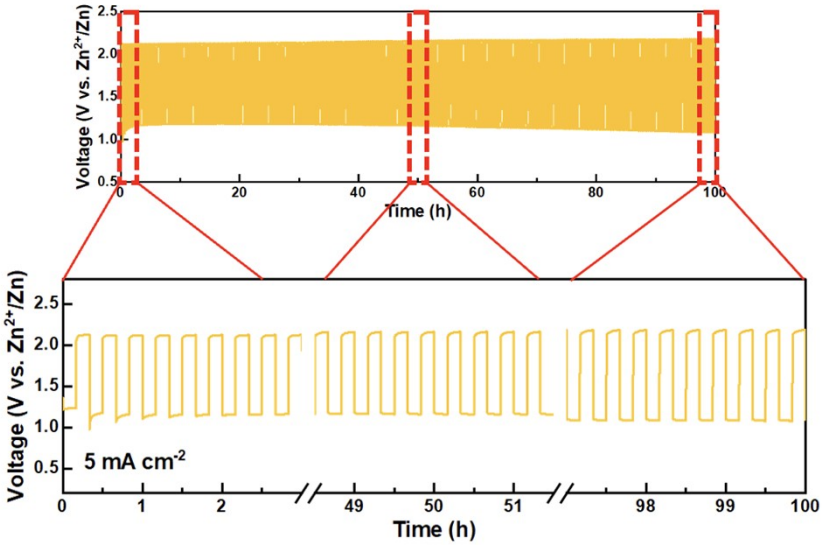

Fig. S20 Long-term galvanostatic cycling at 5 mA cm^{-2} of zinc-air batteries based on N-doped carbon/FeCoCu-15 ORR electrocatalysts.

Table S8 Comparison of typical parameters of this work with reported Zn-air batteries.

ORR catalyst	Loading (mg cm^{-2})	Open Circuit Voltage (V)	Specific Capacity (mAh g^{-1})	Energy Density (Wh kg^{-1})	Peak Power Density (mW cm^{-2})	Durability (h)	Ref.
N-doped carbon/FeCoCu-15	0.50	1.50	810	918	154.7	900 h at 2 mA cm^{-2}	This work
CoO-TiO_2@NG	–	–	816	–	146.8	110 h	[1]
MnO/NC	1.00	1.39	795	–	146.5	60 h at 5 mA cm^{-2}	[2]
NiCo/Co-NiO/rGO	0.50	1.44	807	969	95.5	140 h at 10 mA cm^{-2}	[3]
ZnSe@PNCs-1000	1.00	1.44	818	–	126	200 h at 5 mA cm^{-2}	[4]
MoC@C	1.00	1.43	796	969	132.2	–	[6]
Cu−N−C	–	1.45	718	–	92.2	150 h at 10 mA cm^{-2}	[7]
CoP/CoO@MNC-CNT	2.00	1.40	725	–	152.8	500 h at 10 mA cm^{-2}	[12]
CoNiPt@C	1.60	1.60	–	–	172	70 h at 10 mA cm^{-2}	[13]
Fe-NP/MNCF		1.48	795	–	111.6	120 h	[14]
Cu-Zn/N-doped carbon	1.00	1.20	606	693	170	–	[15]
Fe-N-C/Nb_4C_3Tx	1.00	1.51	–	–	136	220 h at 5 mA cm^{-2}	[16]
Fe/N-doped carbon	–	1.47	630	–	186.1	60 h at 10 mA cm^{-2}	[17]
$FeNb_2O_6$/NICC	1.00	1.46	–	–	100.6	200 h at 5 mA cm^{-2}	[18]
Fe-Phen-MIL101	1.00	1.58	725	–	125.8	140 h	[19]
H-$CoTe_2$/$NiTe_2$@NCBs	–	1.54	762	–	166.5	300 h at 10 mA cm^{-2}	[20]
ZnCo-ZIF@Zn-MOF-74	–	1.43	848	–	166	155 h at 2 mA cm^{-2}	[21]
Fe@HNC	1.00	1.49	812	–	171.5	130 h at 5 mA cm^{-2}	[22]
Fe_3C/N,S-CNS	1.00	1.42	–	–	163	750 h at 5 mA cm^{-2}	[23]
N-GCNT/FeCo-3	2.00	1.48	872	653	97.6	40 h at 150 mA cm^{-2}	[24]

The (–) symbol signifies that the information has not been reported.

References

1 Q. Ding, Q. Zhang, B. Li, D. Cai and W. Wu, *J Power Sources*, 2025, **625**, 235675.

2 Q. Zhuang, C. Hu, W. Zhu, G. Cheng, M. Chen, Z. Wang, S. Cai, L. Li, Z. Jin and Q. Wang, *RSC Adv*, 2024, **14**, 24031–24038.

3 Y. Wang, J. Qian, J. Zheng, J. Li, A. Sun, J. Xing, L. Liu and Y. Zheng, *J Alloys Compd*, 2024, **1004**, 175821.

4 L. Yang, X. Yao, C. Du, Z. Han, M. Jin, S. Peng, X. Ma, Y. Zhu, M. Zou and C. Cao, *Chemical Engineering Journal*, 2024, **481**, 148598.

5 J. Chen, B. Feng, W. Wang, Y. Liang, W. Zhang, X. Li, C. Li, N. Wang and Z. Shi, *J Alloys Compd*, 2024, **983**, 173878.

6 E. Lv, M. Qin, H. Chen, R. Zhao, C. Hu, H. Yu, H. Zhang, X. Zhang and X. Dong, *J Energy Storage*, 2024, **95**, 112255.

7 W. J. Niu, W. W. Zhao, Y. Y. Yan, C. Y. Cai, B. X. Yu and R. J. Li, *J Colloid Interface Sci*, 2024, **675**, 989–998.

8 K. Bhunia, J. H. Seok, M. Perumalsamy, K. S. Bejigo, V. Elumalai, S. U. Lee and S. jae Kim, *Nano Energy*, 2024, **129**, 109966.

9 N. Khodayar, A. Noori, M. S. Rahmanifar, M. Moloudi, N. Hassani, M. Neek-Amal, M. F. El-Kady, N. B. Mohamed, X. Xia, Y. Zhang, R. B. Kaner and M. F. Mousavi, *Energy Environ Sci*, 2024, **17**, 5200–5215.

10 Y. Chen, X. Kong, Y. Wang, H. Ye, J. Gao, Y. Qiu, S. Wang, W. Zhao, Y. Wang, J. Zhou and Q. Yuan, *Chemical Engineering Journal*, 2023, **454**, 140512.

11 Q. Jing, Z. Mei, X. Sheng, X. Zou, Y. Yang, C. Zhang, L. Wang, Y. Sun, L. Duan and H. Guo, *Chemical Engineering Journal*, 2023, **462**, 14321.

12 H. W. Go, T. T. Nguyen, Q. P. Ngo, R. Chu, N. H. Kim and J. H. Lee, *Small*, 2023, **19**, 2206341.

13 Y. Pan, J. Gao, Y. Li, E. Lv, U. Khan, X. Yang, J. Yao, A. Nairan and Q. Zhang, *Small*, 2024, **20**, 2304594.

14 T. Wang, Q. Zhang, K. Lian, G. Qi, Q. Liu, L. Feng, G. Hu, J. Luo and X. Liu, *J Colloid Interface Sci*, 2024, **655**, 176–186.

15 K. Wu, S. Li, C. Hu, G. Wen, X. Zeng, M. Wang, J. Wang, M. Chu, H. Shang, M. Ye, W. Wang, F. Wu and S. Peng, *Appl Catal B*, 2024, 124288.

16 M. ul Haq, D. H. Wu, Z. Ajmal, Q. D. Ruan, S. Khan, L. Zhang, A. J. Wang and J. J. Feng, *Appl Catal B*, 2024, **344**, 123632.

17 P. Li, J. Wen, Y. Xiang, M. Li, Y. Zhao, S. Wang, J. Dou, Y. Li, H. Ma and L. Xu, *Inorg Chem Front*, 2024, **11**, 5345–5358.

18 L. Zhang, L. L. Liu, J. J. Feng and A. J. Wang, *J Colloid Interface Sci*, 2024, **661**, 102–112.

19 S. Tian, S. Wu, J. Yang, J. Li, X. Sun, X. Wang, X. Wang, X. Xiang, Y. Wang and Q. Yang, *J Alloys Compd*, 2024, **1005**, 176009.

20 M. Liu, Q. Li, X. Xiao, X. Ma, X. Xu, Y. Yin, B. Zhang, M. Ding, J. Zou and B. Jiang, *Chemical Engineering Journal*, 2024, **486**, 150256.

21 C. Lv, B. Li, Y. Ren, G. Zhang, Z. Lu, L. Li, X. Zhang, X. Yang and X. Yu, *Chemical Engineering Journal*, 2024, **495**, 153670.

22 H. Zhang, H. C. Chen, S. Feizpoor, L. Li, X. Zhang, X. Xu, Z. Zhuang, Z. Li, W. Hu, R. Snyders, D. Wang and C. Wang, *Advanced Materials*, 2024, 2400523.

23 Q. D. Ruan, R. Feng, J. J. Feng, Y. J. Gao, L. Zhang and A. J. Wang, *Small*, 2023, **19**, 2300136.

24 C. Y. Su, H. Cheng, W. Li, Z. Q. Liu, N. Li, Z. Hou, F. Q. Bai, H. X. Zhang and T. Y. Ma, *Adv Energy Mater*, 2017, **7**, 1602420.